

# A model of flux regulation in the cholesterol biosynthesis pathway: Immune mediated graduated flux reduction versus statin-like led stepped flux reduction

Steven Watterson<sup>ab#</sup>, Maria Luisa Guerriero<sup>bc1</sup>, Mathieu Blanc<sup>ad</sup>,  
Alexander Mazein<sup>ab</sup>, Laurence Loewe<sup>bc2</sup>, Kevin A Robertson<sup>ab</sup>,  
Holly Gibbs<sup>a3</sup>, Guanghou Shui<sup>e</sup>, Markus R Wenk<sup>e</sup>,  
Jane Hillston<sup>bc</sup> and Peter Ghazal<sup>ab#</sup>

February 6, 2012

<sup>a</sup> Division of Pathway Medicine, University of Edinburgh Medical, Chancellors Building, 49 Little France Crescent, Edinburgh EH16 4SB, Scotland, United Kingdom

<sup>b</sup> Centre for Systems Biology at Edinburgh, CH Waddington Building, The King's Buildings, West Mains Road, Edinburgh, EH9 3JU, Scotland, United Kingdom

<sup>c</sup> School of Informatics, Informatics Forum, 10 Crichton Street, University of Edinburgh, EH8 9AB, Scotland, United Kingdom

<sup>d</sup> Centre for Cardiovascular Science, University of Edinburgh, QMRI, 49 Little France Crescent, EH16 4TJ, Scotland, United Kingdom

<sup>e</sup> Department of Biochemistry and Department of Biological Sciences, National University of Singapore, Singapore 117597

## PRESENT ADDRESSES:-

<sup>1</sup> Systems Biology Ireland, Conway Institute, University College Dublin Belfield, Dublin 4, Ireland

<sup>2</sup> Wisconsin Institute for Discovery, 330 North Orchard Street, University of Wisconsin-Madison, Madison, WI 53715, USA

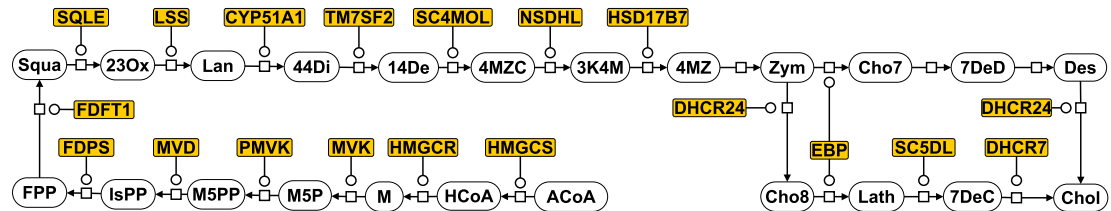
<sup>3</sup> Tissue Microscopy Laboratory, Department of Biomedical Engineering, 337 Zachry Engineering Center, 3120 Texas A&M University, College Station, TX 77843, USA

## # Corresponding authors:-

s.watterson@ed.ac.uk, ph:+44 131 2426242, f: +44 131 2426244

p.ghazal@ed.ac.uk, ph: +44 131 2426242, f: +44 131 2426244

## Graphical Abstract



## Highlights

- We model the cholesterol biosynthesis pathway and its regulation
- The innate immune response leads to a suppression of flux through the pathway
- Statin inhibitors show a different mode of suppression to the immune response
- Statin inhibitor suppression is less robust and less specific than immune suppression

## Abstract

The cholesterol biosynthesis pathway has recently been shown to play an important role in the innate immune response to viral infection with host protection occurring through a coordinate down regulation of the enzymes catalyzing each metabolic step. In contrast, statin based drugs, which form the principle pharmaceutical agents for decreasing the activity of this pathway, target a single enzyme. Here, we build an ordinary differential equation model of the cholesterol biosynthesis pathway in order to investigate how the two regulatory strategies impact upon the behaviour of the pathway. We employ a modest set of assumptions: that the pathway operates away from saturation, that each metabolite is involved in multiple cellular interactions and that mRNA levels reflect enzyme concentrations. Using data taken from primary bone marrow derived macrophage cells infected with murine cytomegalovirus infection or treated with IFN $\gamma$ , we show that, under these assumptions, coordinate down regulation of enzyme activity imparts a graduated reduction in flux along the pathway. In contrast, modelling a statin-like treatment that achieves the same degree of down-regulation in cholesterol production, we show that this delivers a step change in flux along the pathway. The graduated reduction mediated by physiological coordinate regulation of multiple enzymes supports a mechanism that allows a greater level of specificity, altering cholesterol levels with less impact upon interactions branching from the pathway, than pharmacological step reductions. We argue that coordinate regulation is likely to show a long-term evolutionary advantage over single enzyme regulation. Finally, the results from our models have implications for future pharmaceutical therapies intended to target cholesterol production with greater specificity and fewer off target effects, suggesting that this can be achieved by mimicking the coordinated down-regulation observed in immunological responses.

Keywords: Cholesterol, Systems Biology, Regulation, Anti-Viral, Statin

## 1 Introduction

Cholesterol is central to a diverse range of cellular functions, including membrane development and maintenance [1], lipid raft formation and vesicular transport [2], steroid hormone synthesis [3], neurological development [4], and oxysterol and vitamin D synthesis [5]. Recently, the cholesterol metabolism has been shown to have an important role in host-pathogen interactions. It has been documented to be perturbed in response to infection [6, 7] and, conversely, cholesterol and its associated metabolites have been shown to alter inflammatory mediators [8, 9].

Cholesterol synthesis is one step in a pathway of metabolic interactions that is subject to catalytic regulation [10] and evidence suggests that this pathway is critical to the optimal growth of a range of viruses and microbes including cytomegalovirus (CMV), Hepatitis C (HCV), HIV, Japanese Encephalitis (JEV), West Nile (WNV), Dengue (DENV), Measles viruses (MV), African Swine Fever Virus (ASFV), Mycobacteria and Salmonella [6, 7, 11, 12, 13, 14, 15, 16, 17, 18].

The cholesterol biosynthesis pathway itself comprises a sequence of metabolic interactions that occur across several organelles, starting with the processing of Acetyl-Coenzyme A (henceforth denoted ACoA - Supplementary section 1 for a list of all metabolite abbreviations) in the mitochondria and ending with cholesterol synthesis in the endoplasmic reticulum (\*\*cite Mazein et al, same issue\*\*)[?, 19, 20]. This pathway branches in the peroxisome and endoplasmic reticulum, into the sterol arm and the non-sterol arms (prenylation and dolichylation), the latter arms carrying flux away from the main sterol arm.

Coordinate transcriptional control of the enzymes of the cholesterol biosynthesis pathway is mediated by SREBP2 and feedback control occurs through regulation of SREBP2 transport. The SCAP:SREBP2 complex is ordinarily chaperoned to the Golgi complex where SREBP2 is cleaved, before it migrates to the nucleus to activate the suite of enzymes associated with the pathway. However, in the presence of relatively high concentrations of intracellular cholesterol or side-chain hydroxylated cholesterol, in particular 25-hydroxycholesterol, SCAP:SREBP2 is retained instead in the endoplasmic reticulum. Retaining SCAP:SREBP2 acts to down-regulate transcription of the enzymes acting on the pathway until ordinary levels of cholesterol and its derivatives have been restored. Hence, the pathway undergoes transcriptionally mediated regulation through changes to enzyme concentrations [19].

Recently, we reported a modest, but statistically significant, decrement in the concentrations of enzymes associated with cholesterol biosynthesis pathway, in response to both infection and interferon treatment in macrophages. This was observed at the transcriptional level and was shown to correlate with reduced protein concentrations [11]. This decrement was found to be part of the innate immune response, intended to suppress viral growth. However, the mechanism through which such changes decrease the activity of the cholesterol biosynthesis pathway is something that has yet to be fully elucidated in the published literature.

We have sought to investigate this mechanism of regulation, exploring the impact on flux that results from such enzyme decrements. This problem is experimentally challenging, but tractable with computational methods. Flux is the natural quantity to consider when studying metabolic pathway function and flux studies have been employed both theoretically [21, 22] and experimentally [23, 24]. The flux through the pathway describes the stoichiometrically adjusted rate of production of each metabolite and so captures whether and how the production rate of the metabolites affect each other. Ultimately, the final flux value in the pathway describes the rate of cholesterol synthesis. Metabolic Control Analysis (MCA) and Flux Balance Analysis (FBA) are two typical approaches to studying flux in a pathway system. However, MCA approaches focus on the effects of individual infinitesimal changes in enzyme activity rather than the compound effects of multiple finite changes and FBA, in its standard form, does not relate flux changes to substrate concentration changes. As a result, they are inappropriate for our study in which we validate the pathway model at the level

of the substrate, implement multiple finite enzyme decrements and model the effects of chemical inhibition. We build an ordinary differential equation (ODE), dynamical model of the sterol pathway using Michaelis-Menten and mass action kinetics that incorporates additional interactions to represent the consumption of metabolites in non-sterol related processes. We demonstrate that multiple small decreases in enzyme activity can suppress the flux through the main cholesterol biosynthesis pathway. This suppression presents itself as a graduated reduction when the profile of flux is considered.

Cholesterol levels have also been demonstrated to be an important risk factor in cardiovascular disease [25, 26] and their control is an active area of research [27]. Current therapies involve the use of statins to competitively inhibit the enzyme HMGCR which is responsible for catalysis of the interaction transforming 3-hydroxy-3-methyl-glutaryl Coenzyme A (HCoA) to Mevalonate (M). However, the efficacy of such therapies is limited by drug toxicity and off target effects [28, 29, 30]. Here, we show that statin treatment regulates the flux through the pathway in a manner that is markedly different to that following infection. The metabolic interaction catalyzed by HMGCR is significantly upstream of cholesterol biosynthesis and we show that the impact of a statin-like treatment is to suppress flux throughout most of the pathway. This impacts significantly upon many of the metabolites upstream of cholesterol and upon the non-sterol arms, thereby incurring off-target effects. In contrast, because coordinate enzyme regulation leads to a graduated reduction in flux along the pathway, it has a less dramatic impact upon the branches upstream of cholesterol production.

This manuscript is organized as follows. In Section 2, we describe the experimental and mathematical methods employed to determine enzyme and metabolite levels in response to infection and IFN $\gamma$  treatment and to model the pathway. In Subsection 2.1, we describe the experimental method and in subsections 2.2 and 2.3, we describe how the model was built, how the initial conditions were defined and how the model was used to simulate pathway activity. In Section 3, we present the results of using the model to study the flux through the pathway, with subsections 3.1, 3.2, 3.3 and 3.4 describing the validation of the model and the impact on the flux of the response to IFN $\gamma$  treatment, to CMV infection and to statin intervention, respectively. In Section 4, we discuss these results, their relationship, their off-target effects and their implications for specific, targeted regulatory strategies. In Section 5, we summarize our results. Supplementary material in support of the results presented here is available online.

## 2 Materials & Methods

### 2.1 Experimental measurements

Enzyme levels were inferred from gene expression measurements of bone-marrow derived macrophage cells in two time course experiments, one in which cells were infected with murine cytomegalovirus (mCMV) and one in which cells were treated with IFN $\gamma$ . Measurements were taken at half hour intervals for 12 hours using Agilent microarray platforms and at 24 hours for select members using QPCR. Agreement between mRNA expression and protein concentrations was validated by quantitative western blotting for selected members [11].

Intracellular cholesterol concentration was determined enzymatically using the Amplex-Red cholesterol assay kit (Molecular Probes) according to manufacturer recommendations. Briefly, cells were washed with 1 ml ice cold PBS and then lysed in 200  $\mu$ l cold Lipid buffer containing 0.5M of potassium phosphate, pH 7.4, 0.25 mM cholic acid, and 0.5% triton X-100. Cell lysates were sonicated on ice with three 10-second pulses at high intensity. 20  $\mu$ l were then used to determine protein concentration using a standard BSA assay to normalize the protein concentration. For cholesterol measurement, 20  $\mu$ l of each sample were added

to 80  $\mu$ l assay solution, which contained 300  $\mu$ M Amplex Red reagent, 2 U per ml HRP and 2 U per ml cholesterol oxidase, 0.1M of potassium phosphate, pH 7.4, 0.05mM cholic acid, and 0.1% triton X-100. After preincubation for 30 min at 37 °C under light exclusion conditions, fluorescence was measured using excitation at 530±2.5 nm and fluorescence detection at 590±2.5 nm with a Polarstar Optima Multifunction Microplate Reader (BMG Labtech, UK). The values were corrected from the background. The relative amount of free cholesterol to the mock treated samples was calculated using the manufacturer's supplied standard curve.

For the measurement of metabolite concentration, an Agilent high performance liquid chromatography (HPLC) system coupled with an Applied Biosystem Triple Quadrupole/Ion Trap mass spectrometer (4000Qtrap) was used for quantification of individual polar lipids (phospholipids and sphingolipids). Electrospray ionization-based multiple reaction monitoring (MRM) transitions were set up for the quantitative analysis of various polar lipids. HPLC atmosphere chemical ionization (APCI)/MS were carried out for analysis of sterols [11].

## 2.2 Model Construction

Because regulation and feedback occur through transcriptional control of enzyme activity, we chose to model the impact of enzyme activity on the pathway flux. This obviated the need to explicitly consider SREBP2 mediated feedback in the pathway as any feedback would be accounted for in our measurements of enzyme activity. From the representations available in the KEGG pathway database [10], we assembled the description of the pathway shown in Fig. 1A (presented in SBGN notation [31]). From this description, we built a deterministic model of the pathway in which catalyzed metabolic transitions were described with Michaelis-Menten kinetics and the autocatalyzed metabolic transitions were described with mass action kinetics. Metabolites play a role in a range of cellular processes and undergo degradation. To capture this each metabolite was also considered to be consumed in an interaction competing with the main pathway, but at a rate lower than its consumption in the main pathway. The competing reactions were modelled with mass action kinetics (not shown in Fig. 1A).

Parameter values for the cholesterol biosynthesis pathway were taken from the Brenda enzyme database [32]. Where parameters were not known, they were approximated with the mean of the corresponding known parameters. The mean values were  $\bar{k}_{cat} = 7.9 * 10^3 \text{hr}^{-1}$  and  $\bar{k}_m = 4.2 * 10^{-2} \text{mM}$ . Normalized enzyme levels were inferred from the microarray time courses described above. To obtain an absolute scale for these measurements, we assumed an average number of 5000 enzyme proteins [33] in a region of the cell (the *endoplasmic reticulum*) of volume  $10^{-14} \text{l}$  [34, 35, 36]. This gave a concentration scale of  $\bar{E} = 8.3 * 10^{-4} \text{mM}$  which we took to correspond to the mean normalized enzyme level measurement across both experiments at the start of each time course (mean normalized measurement = 1279.2). We subsequently transformed the normalized expression levels to concentrations using this equivalence and took expression levels to be commensurate with protein levels following the validation described above.

From Supplementary section 2, we can see that, in the limit of low substrate, a Michaelis-Menten interaction acts much like a mass action interaction with a rate constant  $k = k_{cat}E/k_m$ , where  $E$  is the enzyme concentration. Using  $\bar{k}_{cat}$ ,  $\bar{k}_m$  and  $\bar{E}$ , this gave  $k = 156 \text{hr}^{-1}$  and we used this value as the rate constant for all the autocatalyzed, mass-action interactions in the main pathway.

In order for the behaviour of the cholesterol biosynthesis pathway activity to dominate over the other dynamical effects, the competing interactions were taken to have mass action rate constants two orders of magnitude smaller than the corresponding mass action constants formed from the main pathway parameters. Thus, for substrate  $i$ , consumed in a Michaelis-Menten interaction, the corresponding mass action constant

would be  $k_{cat}^i E_0^i / k_m^i$  and we assigned to the mass action constant of the competing interaction the value  $k_{cat}^i E_0^i / (100k_m^i)$ , where  $k_{cat}^i$  and  $k_m^i$  are the turnover and Michaelis-Menten constants of the Michaelis-Menten pathway interaction consuming the metabolite and  $E_0^i$  is the enzyme concentration at the start of the time course. Cholesterol was assumed to be consumed at the same rate that it was created in order to avoid accumulation.

A complete list of parameter values is shown in Supplementary sections 3 and 4 and a complete list of normalized enzyme measurements is shown in Supplementary sections 5 and 6.

### 2.3 Modelling strategy

Near saturation, small fluctuations in enzyme concentration lead to small changes of  $V_{max}$  in Michaelis-Menten interactions ( $V_{max} = k_{cat} \times \text{enzyme concentration}$ ) and this, in turn, leads to large changes in metabolite concentration. Hence, we would expect the pathway to operate in a regime away from saturation where the dynamics would be more stable and robust. Here, we assumed that the pathway was operating away from saturation of the Michaelis-Menten interactions.

We assumed a level of flux into the pathway  $\sim 2/3$ rds of the lowest  $V_{max}$  value obtained across both time courses. From the parameters and the enzyme concentrations at the start of each time course, we calculated the concentrations of each metabolite that would allow the pathway to continue in dynamic equilibrium if no changes were observed in the enzyme concentrations (see Supplementary section 7). The pathway was then numerically integrated, allowing the enzyme concentrations to change in accordance with the concentrations measured in the time course. In the interval between time points, enzyme concentrations were calculated through linear interpolation.

In each interaction of the pathway, the flux was defined and calculated as the rate at which each metabolite is produced. Because this pathway is stoichiometrically trivial, this allowed a direct comparison between all interactions in the pathway. Numerical integration of the pathway was conducted in a two step process, with all the fluxes  $\vec{f}(t)$  being calculated from metabolite concentrations and then all the metabolite concentrations being updated from the net fluxes. For a general interaction in the interior of a sequential pathway the update rule took the form  $m_i(t + \Delta t) = m_i(t) + (f_{i-1}(t) - f_i(t))\Delta t$ , where  $m_i$  is the concentration of metabolite  $i$ . Modifications to this rule were required at branch points in the pathway and at the start and end. In order to determine a size for  $\Delta t$ , simulations were run in iterations, with values for  $\Delta t$  progressively decreasing. Iterations continued until a value for  $\Delta t$  was reached at which the results stabilized with no variation in the first four significant figures of the pathway output. This determined the  $\Delta t$  size.

## 3 Results

### 3.1 Model validation

Our first step was to assess the quality of the model by testing whether it behaved in a manner consistent with the observed underlying biology. We did this by comparing the concentrations of three metabolites that cover the pathway at 12 hours following immune challenge.

In Figs.1B-D, we see normalized metabolite concentrations at 0 and 12 hours following mCMV infection or following IFNy treatment, from both experiment and simulation. Experimentally determined concentrations were normalized against the mock treatment time course; computationally determined concentrations were normalized against the concentration calculated at the start of the time course, determined as part of the initial conditions (see section 2.2).

From a comparison of the experimental and the computationally determined values, we can see that the behaviour of the model is in qualitative agreement with the experimentally observed response of the macrophage cells to mCMV infection and IFN $\gamma$  treatment. This agreement becomes even clearer if we consider the values at 0, 12 and 24 hours post infection or post treatment (Supplementary Fig. 1). This gives us confidence that the model can be used to address questions surrounding the relationship between changes in enzyme levels, metabolite concentrations and flux.

### **3.2 In response to IFN $\gamma$ treatment, the flux through the cholesterol biosynthesis pathway is significantly suppressed in a graduated manner**

It is not known how coordinate enzyme control impacts upon flux through the pathway and cholesterol biosynthesis. Thus, we first chose to assess the response of the pathway to the enzyme time courses measured following IFN $\gamma$  treatment.

We simulated the pathway activity by taking the measurements from the microarray time course of macrophage cells following IFN $\gamma$  treatment to represent enzyme concentrations (we have previously shown good correlation between mRNA concentrations and enzyme levels [11]). Fig. 2A shows the resulting profile of flux along the pathway and how this profile develops over the 12 hours. For presentational purposes, we numbered the interactions with 1 representing the input flux and 17 representing cholesterol synthesis (for the full numbering, see Supplementary section 12). The pathway forks at Zymosterol with flux split down both forks. Cholesterol synthesis occurs on both forks and for presentational simplicity, we omitted the details of each fork, but retained the cholesterol synthesis rate, calculated as the sum of the synthesis rates from each fork.

From Fig. 2A, we can see that the profile of flux is relatively constant across the pathway at the point of treatment, but that, as time advances, the flux along the pathway becomes suppressed, leading to a much reduced rate of cholesterol synthesis at 12 hours post treatment.

In order to explore the down-regulation in pathway activity further, we examined the cross sections taken at 0 and 12 hours post treatment. The resulting profiles are shown in Fig. 2B. At the point of treatment (0 hrs), we can see that the pathway undergoes a very modest reduction in flux along its length, attributable to the flux lost through the interactions competing for each metabolite. However, as a result of the coordinate down regulation of enzyme activity across the time course, this modest reduction is dramatically amplified.

This profile of flux reduction along the pathway can be considered in terms of (a) dominant interactions, in which the flux reduces significantly and (b) non-dominant interactions, in which the flux reduces more modestly. From Fig. 2B, we can see that the dominant interaction is Squalene-2,3Oxidosqualene (henceforth Squa-23Ox). In order to further explore the degree of suppression in pathway flux that takes place in the non-dominant interactions, we investigated the profile of flux leading up to Squa synthesis and from Squa to 3-keto-4-methyl-zymosterol (henceforth 3k4m), normalizing the flux values against the flux through the first interaction in the sequence. The flux profiles are shown in Figs. 2C and 2D, respectively. In both Figs. 2C and 2D, we can see that the flux through the sequence of interactions is significantly suppressed after 12 hours.

### **3.3 In response to mCMV infection, the flux through the cholesterol biosynthesis pathway shows some suppression in a graduated manner**

Ligand activation of the IFN $\gamma$  gamma receptor by the IFN $\gamma$  cytokine is involved in immune activation of macrophages. To compare modulation of the pathway in response to IFN $\gamma$  with its modulation in response

to infection, we next modelled the pathway activity using the time course recorded in response to mCMV infection. Fig. 3A shows the resulting profile of flux along the pathway and how this profile developed over time. As in Fig. 2, we numbered the interactions with 1 representing the input flux and 17 representing cholesterol synthesis (see Supplementary section 12). Because the pathway forks at Zymosterol, we omitted the details of the flux along each fork, but retained the cholesterol synthesis rate, calculated as the sum of the synthesis rates on each fork.

The profile of flux in Fig. 3A is relatively constant across the pathway at the moment of infection, but as time increases, the flux along the pathway reduces, leading to a suppressed pathway and a much reduced rate of cholesterol synthesis. To analyze this response further, we again took cross sections from this surface at 0 and 12 hours post infection. In Fig. 3B, we can see that there is a modest reduction in flux at the point of treatment (0 hours) and that this is amplified as a result of the response to treatment.

As mentioned previously, the profile of flux reduction along the pathway can be considered in terms of interactions that make a dominant contribution to flux reduction and those that make a non-dominant contribution. Interestingly, we see that the distribution of dominant interactions is distinct from the distribution seen in the response to IFN $\gamma$  treatment. Here, the dominant interactions are ACoA-HCoA and Squa-23Ox. In order to explore further the regulation of flux through the non-dominant interactions, we examined the flux profiles between dominant interactions, normalizing the flux through each sequence against the flux through the first interaction in the sequence. The results can be seen in Figs. 3C and D. In the first of these profiles, it is clear that the flux at 12 hours post infection is similar to that at infection, but that some modest reduction does occur towards the end of the sequence as a result of the enzyme regulation. In the second profile, the flux profile clearly does not alter significantly between 0 hours and 12 hours post infection.

### 3.4 Under statin-like intervention, the pathway acquires a step reduction in flux

From Figs. 2 and 3, we can see that the pathway has the ability to respond to perturbation throughout its length. We chose to compare these flux profiles to that which is likely to be obtained when statin-like inhibitors that target the HMGCR enzyme are introduced into the pathway.

Fig. 4A shows the profile of flux obtained in the unperturbed pathway and the profiles at 12 hours following IFN $\gamma$  treatment and mCMV infection. Fig. 4A also shows the profile of flux obtained when the statin-like inhibitor is introduced with a concentration sufficient to suppress cholesterol production to the mean of the production rates for IFN $\gamma$  treatment and mCMV infection at 12 hours. Here we can see that the profile takes a very different form, impacting dramatically upon the interactions upstream of Squa. The profile corresponding to statin-like inhibition is less graduated than in the physiological responses both in terms of the dominant interactions and the non-dominant interactions, and such a flat profile arises because the single HMGCR inhibited interaction takes the entire regulatory burden of reducing the flux along the pathway with the other interactions contributing no more flux reduction than in the unperturbed case.

## 4 Discussion

Figs. 2, 3 and 4 give us insight into how the cholesterol biosynthesis pathway operates and its various modes of regulation. Fig. 2 shows that, in response to IFN $\gamma$  treatment, the pathway undergoes a reduction in flux that is mediated by both the dominant and non-dominant interactions. The distribution of flux at the point of IFN $\gamma$  treatment shows a very mild reduction along the pathway. This is attributable to the flux lost through the off-pathway, competing interactions. However, at 12 hours post treatment, we can see that the flux becomes significantly suppressed along the pathway due to the coordinate enzyme reduction. This

occurs because a reduction in the enzyme concentration in an interaction has the effect of decreasing the rate of the interaction. This, in turn, increases the proportion of flux shunted through the off-pathway interaction competing for the same metabolite. At 12 hours post treatment, we can see that most of the interactions on the pathway play a suppressive role. This implies that, for most of the metabolites, there is an increase in the proportion of flux shunted through the off-pathway interactions, if flux conservation is to be maintained.

In Fig. 3, we can see that the pathway also undergoes a reduction in flux in response to mCMV infection. In this case, the reduction is mediated mostly by the dominant interactions with very few non-dominant interactions contributing to the suppression of flux between 0 and 12 hours post infection. Here, we infer that the coordinate enzyme control leads to an increased proportion of flux being shunted through the off-pathway interactions that compete for metabolites with the dominant interactions. However, we see little suppression of flux through the non-dominant interactions between 0 and 12 hours post infection, implying that the proportion of flux being shunted through the off-pathway interactions, competing for the same metabolites, stays approximately the same as at the point of infection.

In Fig. 4A, we see that a statin-like pharmaceutical intervention comparable to the immune-led responses introduces a profile of flux with a significantly different shape to that of the immune led response. A statin-like intervention leads to a step down in flux towards the start of the pathway with the result that the flux passing through many of the interactions in the upper half of the pathway is significantly lower than the levels observed in immune-led responses. We can infer that a statin-like intervention shunts a significantly increased proportion of flux through the off-pathway interaction competing for HCoA. In the remaining interactions, no significant change in the proportion of flux passing through the main pathway interactions occurs.

If we consider the flux profiles shown in Fig. 4A, we see that the introduction of a statin-like inhibitor steps down the flux at the interaction HCoA-M and that this has consequences for many of the interactions downstream of HCoA-M. In the upper regions of the pathway, the level of flux after the introduction of a statin-like inhibitor is well below that achieved in immune-led responses. This is particularly significant for the interactions that consume and produce Isopentyl-PP (IsPP) and Farnesyl-PP (FPP) as these metabolites are also consumed in the prenylation and dolichylation non-sterol arms that fork from the main sterol pathway (\*\*cite Mazein et al, same issue\*\*)[?, 19, 20]. Hence, the difference in profiles between statin-like intervention and the immune-led regulation is likely to have significant consequences for these non-sterol arms due to the difference in flux passing through the branch point in the pathway. Off target effects are known to be a particular concern for statin based treatments [30, 29] and the difference in flux profiles may provide a clue as to why this is the case.

If we consider the profiles of flux associated with coordinate enzyme regulation and with single enzyme regulation, it is clear that the coordinate regulation provides a more robust strategy for regulating the pathway. Single enzyme regulation offers no protection against metabolite surges occurring downstream of the regulated interaction. Therefore, distributing flux reduction over multiple interactions, rather than a single interaction, protects the regulatory mechanism from cellular perturbations. The regulation of the cholesterol biosynthesis pathway by IFN $\gamma$  has been shown to be part of an antiviral response and a distributed flux reduction also increases the difficulty for a pathogen to manipulate the pathway to proviral effect. For these reasons, it is likely that coordinate control has enjoyed a selective advantage in the evolution of immune regulation.

From Figs. 2 and 3, we can see that all the interactions have the potential to play a regulatory role. Therefore, an important question to ask is whether a combination of inhibitors can be chosen such that the flux reduction is distributed evenly throughout the pathway. Such a regulatory structure would be optimally

robust. This could be achieved through control at the transcriptional level, tuning SREBP2 activity, or at the enzyme level using pharmaceutical inhibition or miRNA induced degradation. Such an arrangement can be achieved in the models described above by using the combination of inhibitors with levels described in Supplementary section 9. The resulting flux profile is shown in Fig. 4B. Here, the inhibitor concentrations have been chosen so that, for each metabolite, the proportion of flux shunted down the off-pathway interaction to flux continuing down the main pathway is the exactly same. In addition to the superior robustness of such a distributed regulation, this profile of flux would also show greater specificity than a stepped, statin-like treatment as the upstream interactions would be significantly less flux suppressed, reducing the impact on off-pathway interactions. It is possible to speculate that a regulatory arrangement that targets a single interaction towards the end of the pathway would demonstrate even greater specificity to cholesterol as it would create a flux profile in which the flux remains at unregulated levels for most of the pathway, but steps down immediately before the point of cholesterol synthesis. However, such a regulatory structure would not enjoy the robustness of multiple interaction regulation. The improved specificity and robustness that comes with multiple interaction regulation suggests that future pharmacological therapies may be able to act more efficiently and with fewer side effects, if they are designed either to mimic the physiological response of IFN $\gamma$  treatment or to create a distributed regulation of flux comparable to Fig. 4B.

Further interesting detail can be observed when we allow our simulations to run up to 24 hours post infection or post IFN $\gamma$  treatment. At 24 hours we had access to only a limited number of QPCR measurements for a subset of the enzymes on the pathway, so to provide values for the unmeasured enzymes at 24 hours, we assumed that the concentration did not change from the 12 hour time point. From Supplementary Fig. 1, we can see that qualitative agreement between our simulated metabolite levels and the measured values improves in the 12-24 hour window, further supporting the use of this model to explore the dynamics of the cholesterol biosynthesis pathway. Exploring the flux profiles at 24 hours post IFN $\gamma$  treatment and post mCMV infection (Supplementary Figs. 2 and 3, respectively), we can see that there is a difference in the relative timing of the flux suppression. In mCMV infection, pathway flux is suppressed at 12 hours post infection and continues to be further suppressed over the 12 to 24 hour interval. However, in response to IFN $\gamma$  treatment, we see that the pathway starts to recover its pretreated profile of flux in the 12 to 24 hour window. The simplest explanation for this difference would be that there is an inherent delay between mCMV infection and the induction of IFN $\gamma$  signalling within cell populations. This would predict that running the mCMV infection experiments for a longer duration would yield enzyme expression measurements that would lead to a rise in pathway flux similar to that observed in IFN $\gamma$  treatment. Although at 12 hours post mCMV infection there was little evidence of the non-dominant interactions contributing to pathway regulation, it is also worth noting that, at 24 hours post mCMV infection, the non-dominant interactions start to show a modest suppression of flux comparable to that seen in the 0-12 hour window following IFN $\gamma$  treatment. This further supports the idea that the two profiles are related.

The flux profiles shown in Figs. 2A and 3A and in Supplementary Figs. 2A and 3A exhibit interesting features. The broad trend is towards pathway suppression. However, there are points at which the flux exceeds unperturbed levels and where the flux downstream exceeds the flux into the pathway. This may be attributable, at least in part, to technical noise in the time course microarray measurements. However, we cannot rule out that this is biological. Points where the flux consuming a metabolite exceeds the flux producing it correspond to a reduction in the concentration of a metabolite (data not shown). In Figs 2B and 3B, we see that there is a rise in flux at the 3K4M-4MZ interaction. In our simulations, this corresponded to a reduction in the concentration of 3K4M (data not shown).

Making quantitative predictions of pathway function requires a comprehensive set of high confidence

parameters. Without such a parameter set, we are restricted to qualitative observations. Despite the importance of the cholesterol biosynthesis pathway to innate immunity and cardiovascular health and despite its value to industry as the target pathway of the statin class of drugs, we can see from the Table in Supplementary section 3 that the parameterization of this pathway is largely incomplete. This is a surprising result. The lack of a rigorous parameterization impedes studies of pathway behaviour and the development of more advanced scientific and therapeutic interventions. The incomplete nature of the parameterization led us to use estimates for the unknown parameters and this has implications for the flux profiles we obtained in simulations. The particular arrangement of dominant interactions and non-dominant interactions, for example, is parameter dependent and we can see from Supplementary section 3 that the two interactions identified as playing a dominant role in flux reduction (ACoA-HCoA and Squa-23Ox) are those with the lowest turnover ( $k_{cat}$ ) values. Accurate predictions of the precise arrangement of dominant and non-dominant interactions require a complete, high confidence parameter set. However, under the assumptions made in the model, it is a parameter independent result that all the interactions can contribute a modulation of flux.

The coordinate down regulation of enzyme activity has been demonstrated to be an innate, immune, anti-viral response to mCMV infection mediated by IFN $\gamma$ , rather than a pathogenic intervention [11] and so it would appear that flux reduction is also part of the innate immune response. The cholesterol biosynthesis pathway has been demonstrated to be critical to the optimal viral infection of a further range of viruses (Hepatitis C (HCV), HIV, Japanese Encephalitis (JEV), West Nile (WNV), Dengue (DENV), Measles viruses (MV) and African Swine Fever Viruses (ASFV) [6, 7, 11, 12, 13, 14, 15, 18]). Since the flux suppression is in response to IFN $\gamma$ , a general immunological cytokine, it is possible that such a flux suppression might be part of a general antiviral response.

## 5 Conclusion

Here, we have shown, with a simple dynamical model, that the coordinate down regulation of the enzymes in the cholesterol biosynthesis pathway in macrophages, observed in response to mCMV infection and IFN $\gamma$ , treatment leads to a graduated reduction in flux along the pathway that can be considered in terms of dominant interactions that significantly suppress the flux and non-dominant interactions that make modest, but not insignificant contributions to flux suppression. The model was built using a combination of Michaelis-Menten and mass action interactions and was validated using experimental measurements of metabolite concentrations at a range of time points. Our result suggests that all the interactions in the pathway could be candidate intervention points for future therapeutic strategies.

We were able to compare the impact on flux of coordinate regulation which acts to regulate multiple interactions to the impact of statin-like inhibitors which regulate a single enzyme. This allowed us to explore the advantages of multiple interaction regulation over single enzyme regulation. The graduated profile generated by coordinate regulation enjoys greater robustness and greater specificity and we highlight the importance of this for the prenylation and dolichylation non-sterol arms that fork from the cholesterol biosynthesis pathway. We suggest that such a multiple interaction regulation could be exploited in future pharmaceutical therapies in order to improve their efficacy and specificity, perhaps mimicking the regulation of the pathway observed in immunological responses.

## 6 Acknowledgments

This work was supported by the Wellcome Trust (WT066784) programme grant and BBSRC to PG. The Centre for Systems Biology at Edinburgh is a centre for Integrative Systems Biology supported by the BBSRC and EPSRC (BB/D019621/1).

## 7 Author Contribution

AM, SW, HG, KAR and PG compiled a description of the cholesterol biosynthesis pathway. SW, MLG, JH and PG modelled the pathway. SW, LL and MLG compiled parameters for the pathway. MB, GS and MRW completed the experiments. Analysis was completed by SW and PG. SW, KAR and PG wrote the manuscript with feedback from all authors.

## References

- [1] Röper K, Corbeil D, Huttner WB. Retention of prominin in microvilli reveals distinct cholesterol-based lipid micro-domains in the apical plasma membrane. *Nat Cell Biol.* 2000 Sep;2(9):582–92.
- [2] Simons K, Ehehalt R. Cholesterol, lipid rafts, and disease. *J Clin Invest.* 2002 Sep;110(5):597–603.
- [3] Miller WL. Molecular biology of steroid hormone synthesis. *Endocr Rev.* 1988 Aug;9(3):295–318.
- [4] Dietschy JM, Turley SD. Cholesterol metabolism in the brain. *Curr Opin Lipidol.* 2001 Apr;12(2):105–12.
- [5] Holick MF. Vitamin D: a D-Lightful health perspective. *Nutr Rev.* 2008 Oct;66(10 Suppl 2):S182–94.
- [6] Rothwell C, Lebreton A, Ng CY, Lim JYH, Liu W, Vasudevan S, et al. Cholesterol biosynthesis modulation regulates dengue viral replication. *Virology.* 2009 Jun;389(1-2):8–19.
- [7] Robinzon S, Dafa-Berger A, Dyer MD, Paeper B, Proll SC, Teal TH, et al. Impaired cholesterol biosynthesis in a neuronal cell line persistently infected with measles virus. *Journal of Virology.* 2009 Jun;83(11):5495–504.
- [8] Yvan-Charvet L, Wang N, Tall AR. Role of HDL, ABCA1, and ABCG1 transporters in cholesterol efflux and immune responses. *Arterioscler Thromb Vasc Biol.* 2010 Feb;30(2):139–43.
- [9] Zhu X, Lee JY, Timmins JM, Brown JM, Boudyguina E, Mulya A, et al. Increased cellular free cholesterol in macrophage-specific Abca1 knock-out mice enhances pro-inflammatory response of macrophages. *J Biol Chem.* 2008 Aug;283(34):22930–41.
- [10] Kanehisa M, Goto S, Furumichi M, Tanabe M, Hirakawa M. KEGG for representation and analysis of molecular networks involving diseases and drugs. *Nucleic Acids Res.* 2010 Jan;38(Database issue):D355–60.
- [11] Blanc M, Hsieh WY, Robertson KA, Watterson S, Shui G, Lacaze P, et al. Host defense against viral infection involves interferon mediated down-regulation of sterol biosynthesis. *PLoS Biol.* 2011 Mar;9(3):e1000598.

- [12] Owens CM, Mawhinney C, Grenier JM, Altmeyer R, Lee MS, Borisy AA, et al. Chemical combinations elucidate pathway interactions and regulation relevant to Hepatitis C replication. *Mol Syst Biol.* 2010 Jun;6:375.
- [13] del Real G, Jiménez-Baranda S, Mira E, Lacalle RA, Lucas P, Gómez-Moutón C, et al. Statins inhibit HIV-1 infection by down-regulating Rho activity. *J Exp Med.* 2004 Aug;200(4):541–7.
- [14] Lee CJ, Lin HR, Liao CL, Lin YL. Cholesterol effectively blocks entry of flavivirus. *Journal of Virology.* 2008 Jul;82(13):6470–80.
- [15] Medigesi GR, Hirsch AJ, Streblow DN, Nikolich-Zugich J, Nelson JA. West Nile virus entry requires cholesterol-rich membrane microdomains and is independent of alphavbeta3 integrin. *Journal of Virology.* 2008 Jun;82(11):5212–9.
- [16] Gatfield J, Pieters J. Essential role for cholesterol in entry of mycobacteria into macrophages. *Science.* 2000 Jun;288(5471):1647–50.
- [17] Auweter SD, Yu HB, Arena ET, Guttmann JA, Finlay BB. Oxysterol-binding protein (OSBP) enhances replication of intracellular Salmonella and binds the Salmonella SPI-2 effector SseL via its N-terminus. *Microbes and Infection.* 2011 Sep;.
- [18] Quetglas JI, Hernández B, Galindo I, Muñoz-Moreno R, Cuesta-Geijo MA, Alonso C. Small Rho GTPases and cholesterol biosynthetic pathway intermediates in African swine fever virus infection. *Journal of Virology.* 2011 Nov;.
- [19] Mazein A, Watterson S, Gibbs H, Hsieh W, Abdullah MB, Blanc M, et al. Regulation and feedback of cholesterol metabolism. *Nature Precedings.* 2011 Jan;.
- [20] Honda A, Matsuzaki Y. Cholesterol and chronic hepatitis C virus infection. *Hepatol Res.* 2011 Aug;41(8):697–710.
- [21] Kauffman KJ, Prakash P, Edwards JS. Advances in flux balance analysis. *Curr Opin Biotechnol.* 2003 Oct;14(5):491–6.
- [22] Mahadevan R, Edwards JS, Doyle FJ. Dynamic flux balance analysis of diauxic growth in Escherichia coli. *Biophys J.* 2002 Sep;83(3):1331–40.
- [23] van Rijswijk BRBH, Nanchen A, Nallet S, Kleijn RJ, Sauer U. Large-scale <sup>13</sup>C-flux analysis reveals distinct transcriptional control of respiratory and fermentative metabolism in Escherichia coli. *Mol Syst Biol.* 2011 Mar;7:477.
- [24] Zamboni N, Fendt SM, Rühl M, Sauer U. (13)C-based metabolic flux analysis. *Nat Protoc.* 2009 Jan;4(6):878–92.
- [25] Shoulders CC, Jones EL, Naoumova RP. Genetics of familial combined hyperlipidemia and risk of coronary heart disease. *Hum Mol Genet.* 2004 Apr;13 Spec No 1:R149–60.
- [26] Tabas I. Cholesterol in health and disease. *J Clin Invest.* 2002 Sep;110(5):583–90.
- [27] Honey K. Drug designed to raise HDL levels falls down. *J Clin Invest.* 2007 Feb;117(2):282.
- [28] Bellotta S, Paoletti R, Corsini A. Safety of statins: focus on clinical pharmacokinetics and drug interactions. *Circulation.* 2004 Jun;109(23 Suppl 1):III50–7.

- [29] Kaufmann P, Török M, Zahno A, Waldhauser KM, Brecht K, Krähenbühl S. Toxicity of statins on rat skeletal muscle mitochondria. *Cell Mol Life Sci.* 2006 Oct;63(19-20):2415–25.
- [30] Scheetman G, Hiatt J. Dose-response characteristics of cholesterol-lowering drug therapies: implications for treatment. *Ann Intern Med.* 1996 Dec;125(12):990–1000.
- [31] Novere N, Hucka M, Mi H, Moodie S, Schreiber F, Sorokin A, et al. The Systems Biology Graphical Notation. *Nat Biotechnol.* 2009 Aug;27(8):735.
- [32] Chang A, Scheer M, Grote A, Schomburg I, Schomburg D. BRENDA, AMENDA and FRENDA the enzyme information system: new content and tools in 2009. *Nucleic Acids Res.* 2009 Jan;37(Database issue):D588–D592.
- [33] Ishihama Y, Schmidt T, Rappaport J, Mann M, Hartl FU, Kerner MJ, et al. Protein abundance profiling of the *Escherichia coli* cytosol. *BMC Genomics.* 2008 Jan;9:102.
- [34] Krombach F, Münzing S, Allmeling AM, Gerlach JT, Behr J, Dörger M. Cell size of alveolar macrophages: an interspecies comparison. *Environ Health Perspect.* 1997 Sep;105 Suppl 5:1261–3.
- [35] Huber LA, Pfaller K, Vietor I. Organelle proteomics: implications for subcellular fractionation in proteomics. *Circ Res.* 2003 May;92(9):962–8.
- [36] Machalek AZ. Inside the Cell (Chapter 1). NIH Publication. 2005;05-1051.

## 8 Figure Captions

### 8.1 Figure 1

**Figure 1.** A) The cholesterol pathway represented in SBGN notation, starting with the metabolites Acetyl-Coenzyme A (ACoA) and ending in cholesterol synthesis. B)-D) The normalized concentrations of 14-Lanosterol (B), Zymosterol (C) and Cholesterol (D) at 0 hours (solid, black) and 12 hours (diagonal stripes) after mCMV infection and after IFN $\gamma$  treatment. We show results from experiment and simulation. Experimental measurements were normalized against measurements from a mock time course and simulated measurements were normalized against the concentration at 0hrs.

### 8.2 Figure 2

**Figure 2.** The flux through the cholesterol biosynthesis pathway following treatment with IFN $\gamma$ . A) The development of the flux through the pathway in simulation is shown from 0 hrs to 12 hrs following treatment. Interactions are numbered from 1 (the input flux) to 17 (cholesterol production). For the full numbering, see Supplementary section 12. At 0 hrs, the flux through the pathway is relatively constant. However, by 12 hrs the flux has been significantly suppressed along the pathway. B) The profile of flux through the pathway at 0 hrs and 12 hrs following treatment. These profiles represent cross sections of the surface shown in A). The flux is dramatically reduced in the first 12 hrs. Interactions can be classified as dominant (Squa-23Ox) and non-dominant (the remainder) depending on their degree of impact on the pathway flux. C) The flux through the non-dominant interactions between ACoA-HCoA and FPP-Squa, normalized against the flux through the ACoA-HCoA interaction. The flux through these non-dominant interactions is suppressed more modestly than in the dominant interactions. D) The flux through the non-dominant interactions between Squa-23Ox and 4MZC-3K4M normalized against the flux through Squa-23Ox. The flux through these non-dominant interactions is suppressed more modestly than in the dominant interactions.

### 8.3 Figure 3

**Figure 3.** The flux through the cholesterol biosynthesis pathway following infection with mCMV. A) The development of the flux through the pathway in simulation is shown from 0 hrs to 12 hrs post infection. Interactions are numbered from 1 (the input flux) to 17 (cholesterol production). For the full numbering, see Supplementary section 12. At 0 hrs, the flux through the pathway is relatively constant. However, by 12 hrs the flux has been significantly suppressed along the pathway. B) The profile of flux through the pathway at 0 hrs and 12 hrs post infection. These profiles represent cross sections of the surface shown in A). The flux is dramatically reduced in the first 12 hrs following infection. Interactions can be classified as dominant (ACoA-HCoA and Squa-23Ox) and non-dominant (the remainder) depending on their degree of impact on the pathway flux. C) The flux through the non-dominant interactions between ACoA-HCoA and FPP-Squa, normalized against the flux through the ACoA-HCoA interaction. The flux through these non-dominant interactions shows a mild suppression towards the end of the sequence. D) The flux through the non-dominant interactions between Squa-23Ox and 4MZC-3K4M normalized against the flux through Squa-23Ox. The flux through these non-dominant interactions shows no suppression between 0 and 12 hours.

#### **8.4 Figure 4**

**Figure 4.** A) The effect of a statin-like inhibitor on pathway activity. The profile of flux at 0 hrs and 12 hrs following mCMV infection and IFN $\gamma$  treatment together with the profile of flux in an unperturbed cell following the introduction of a statin-like inhibitor which targets the enzyme HMGCR. The effect of a statin-like inhibitor is to step down the flux through the interactions catalyzed by HMGCR. This impacts upon the pathway significantly upstream of the point of cholesterol synthesis and creates a flux profile dramatically different to that which arises from the biological response to mCMV infection or IFN $\gamma$  treatment. B) The profile of flux achieved along the pathway when inhibitors concentrations are chosen so that each interaction contributes equally to the regulation of flux (Inhibitor levels listed in Supplementary section 9).

## 9 Figures

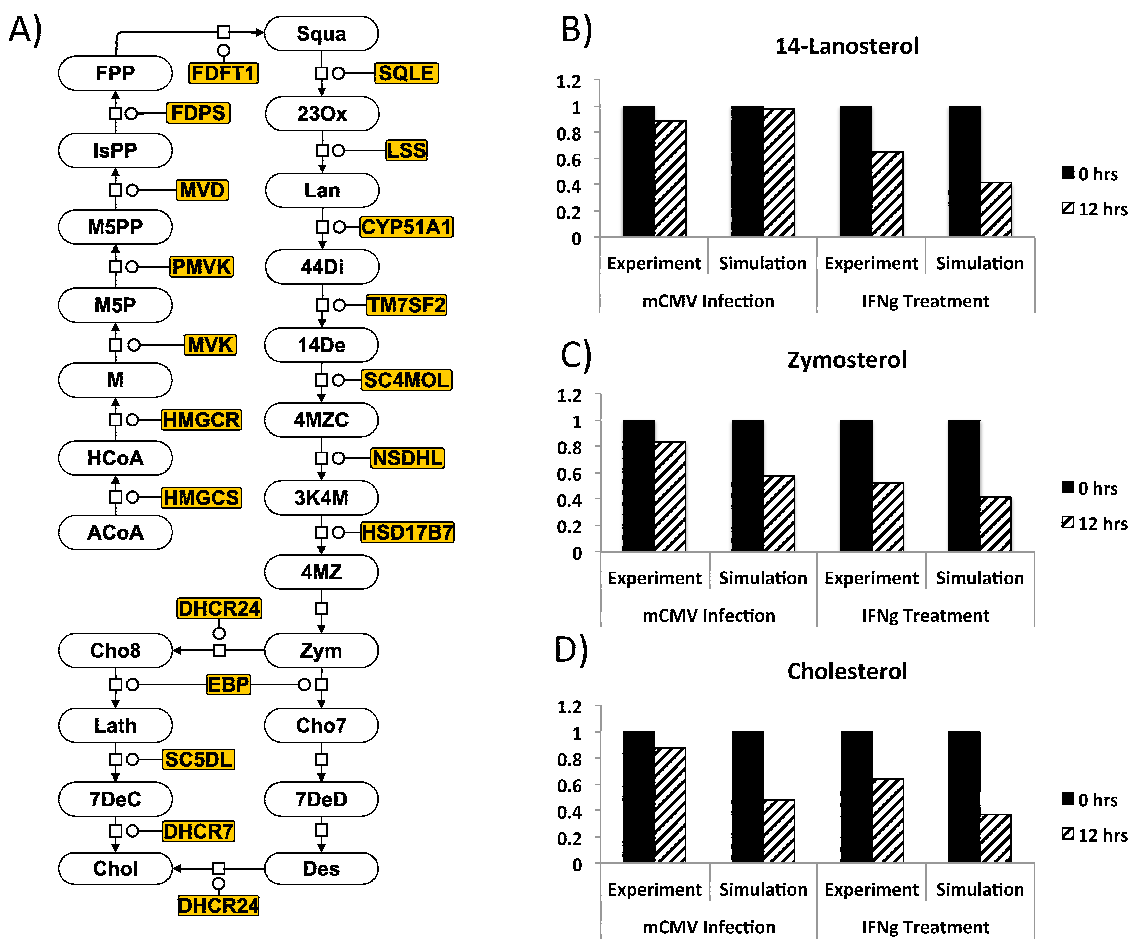


Figure 1:

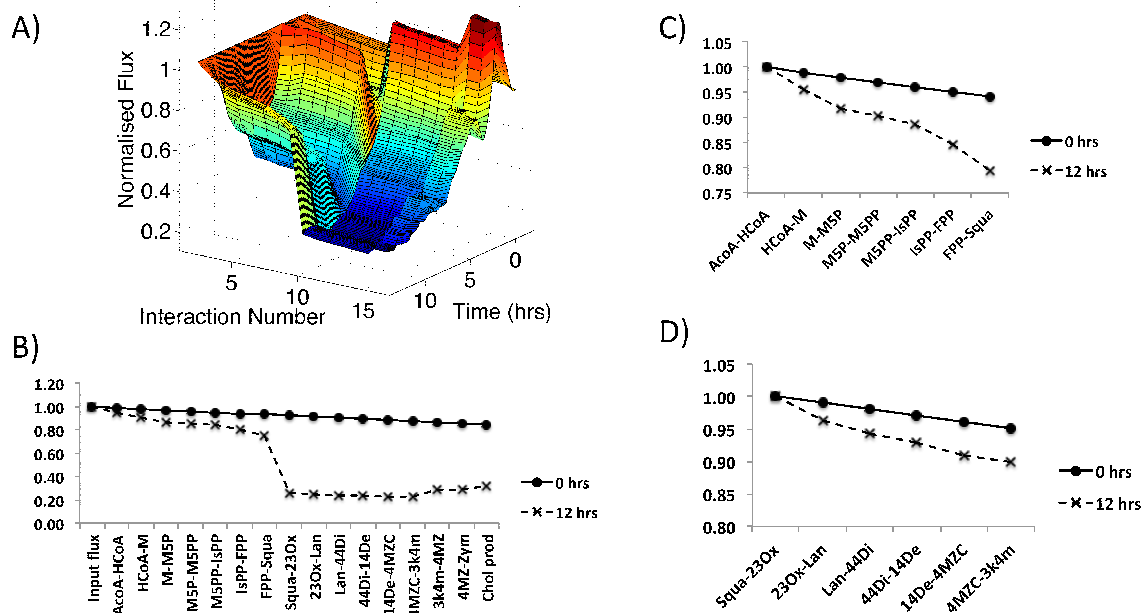


Figure 2:

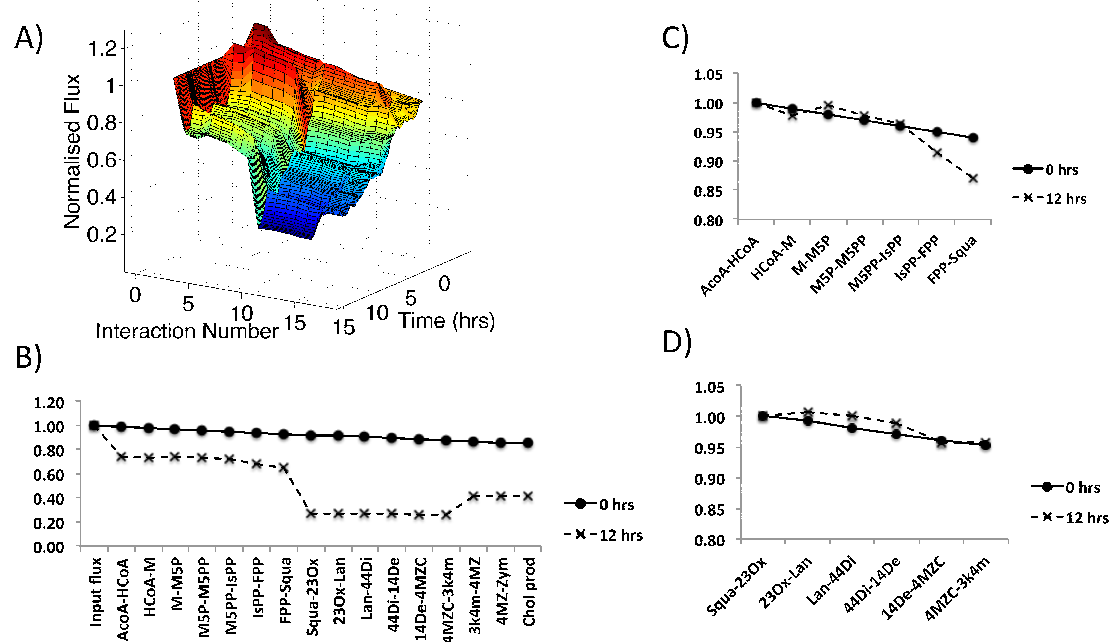


Figure 3:

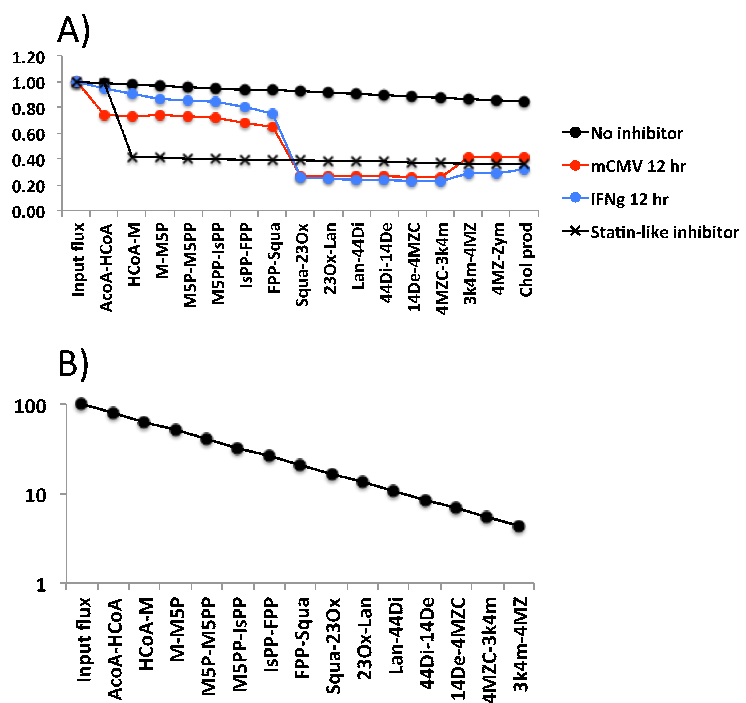


Figure 4:

# Supplementary Material - A model of flux regulation in the cholesterol biosynthesis pathway: Immune mediated graduated flux reduction versus statin-like led stepped flux reduction

Steven Watterson<sup>ab#</sup>, Maria Luisa Guerriero<sup>bc1</sup>, Mathieu Blanc<sup>ad</sup>, Alexander Mazein<sup>ab</sup>, Laurence Loewe<sup>bc2</sup>, Kevin A Robertson<sup>ab</sup>, Holly Gibbs<sup>a3</sup>, Guanghou Shui<sup>e</sup>, Markus R Wenk<sup>e</sup>, Jane Hillston<sup>bc</sup> and Peter Ghazal<sup>ab#</sup>

February 6, 2012

<sup>a</sup> Division of Pathway Medicine, University of Edinburgh Medical, Chancellors Building, 49 Little France Crescent, Edinburgh EH16 4SB, Scotland, United Kingdom

<sup>b</sup> Centre for Systems Biology at Edinburgh, CH Waddington Building, The King's Buildings, West Mains Road, Edinburgh, EH9 3JU, Scotland, United Kingdom

<sup>c</sup> School of Informatics, Informatics Forum, 10 Crichton Street, University of Edinburgh, EH8 9AB, Scotland, United Kingdom

<sup>d</sup> Centre for Cardiovascular Science, University of Edinburgh, QMRI, 49 Little France Crescent, EH16 4TJ, Scotland, United Kingdom

<sup>e</sup> Department of Biochemistry and Department of Biological Sciences, National University of Singapore, Singapore 117597

## PRESENT ADDRESSES:-

<sup>1</sup> Systems Biology Ireland, Conway Institute, University College Dublin Belfield, Dublin 4, Ireland

<sup>2</sup> Wisconsin Institute for Discovery, 330 North Orchard Street, University of Wisconsin-Madison, Madison, WI 53715, USA

<sup>3</sup> Tissue Microscopy Laboratory, Department of Biomedical Engineering, 337 Zachry Engineering Center, 3120 Texas A&M University, College Station, TX 77843, USA

# Corresponding authors:-

s.watterson@ed.ac.uk, ph:+44 131 2426242, f: +44 131 2426244

p.ghazal@ed.ac.uk, ph: +44 131 2426242, f: +44 131 2426244

## 1 Abbreviations used in Fig. 1A.

Acronym	Metabolite
ACoA	Acetyl-CoA
HCoA	HMG-CoA
M	Mevalonate
M5P	Mevalonate-5P
M5PP	Mevalonate-5PP
IsPP	Isopentyl-PP
FPP	Farnesyl-PP
Squa	Squalene
23Ox	2,3 oxydgosqualene
Lan	Lanosterol
44Di	4,4 dimethyl-cholesta-8,14,24-trienol
14De	14-demethyl-lanosterol
4MZC	4-methylzymosterol-carboxylate
3K4M	3-keto-4-methyl-zymosterol
4MZ	4-methylzymosterol
Zym	Zymosterol
Cho7	Cholesta-7,24-dien-3beta-ol
7DeD	7-dehydro-desmosterol
Des	Desmosterol
Cho8	Cholesta-8,en-3beta-ol
Lath	Lathosterol
7DeC	7 dehydro-cholesterol
Chol	Cholesterol

## 2 Relating Michaelis-Menten interactions to Mass-action interactions

For a Michaelis-Menten interaction of the form

$$\frac{dP}{dt} = \frac{k_{cat}ES}{k_m + S}$$

where  $k_{cat}$  is the turnover parameter,  $k_m$  is the Michaelis-Menten constant,  $E$  is the enzyme concentration and  $S$  is the substrate concentration, we want to investigate the consequences of  $S$  being small (ie much less than  $k_m$ ). If we define a small value for  $S$  as  $\Delta S$  (where  $\Delta S \ll k_m$ ), we have

$$\frac{dP}{dt} = \frac{k_{cat}E\Delta S}{k_m + \Delta S}$$

Dividing the numerator and denominator by  $k_m$  gives

$$\frac{dP}{dt} = \frac{\frac{k_{cat}}{k_m}E\Delta S}{1 + \frac{\Delta S}{k_m}}$$

We have  $\frac{\Delta S}{k_m} \ll 1$  and so we can use the identity that

$$\frac{1}{1-x} = 1 + x + x^2 + x^3 + x^4 + \dots \quad \text{for } |x| < 1$$

Thus

$$\frac{dP}{dt} = \frac{\frac{k_{cat}}{k_m}E\Delta S}{1 + \frac{\Delta S}{k_m}} = \frac{k_{cat}}{k_m}E\Delta S \left( 1 - \frac{\Delta S}{k_m} + \left(\frac{\Delta S}{k_m}\right)^2 - \left(\frac{\Delta S}{k_m}\right)^3 + \left(\frac{\Delta S}{k_m}\right)^4 - \dots \right)$$

To second order in  $\Delta S$ , this is

$$\frac{dP}{dt} = \frac{k_{cat}}{k_m}E\Delta S - \frac{k_{cat}}{(k_m)^2}E(\Delta S)^2 + \dots$$

As  $\frac{\Delta S}{k_m} \rightarrow 0$ , all but the first order term make negligible contributions, meaning that

$$\lim_{S \rightarrow 0} \frac{dP}{dt} \approx \frac{k_{cat}}{k_m}ES$$

### 3 Parameters gathered from the Brenda enzyme database and used in our simulations

Interaction	Turnover (hr <sup>-1</sup> ) / (pubmed ID)	Michaelis-Menten Constant (mM) / (pubmed ID)
ACoA-HCoA	33.48/(15233626)	—
HCoA-M	—	0.07/(16128575)
M-M5P	—	0.024/(9325256)
M5P-M5PP	36720/(6248101)	0.025/(9325256)
M5PP-IsPP	17640/(15709780)	0.0074/(9325256)
FPP-Squa	1908/(8239656)	0.0023/(9473303)
Squa-23Ox	65.88/(10666321)	7.7/(10666321)
23Ox-Lan	—	0.015/(1429550)
Lan-44Di	—	0.005/(1567403)
44Di-14De	—	0.0333/(6208195)
4MZC-3K4M	—	0.007/(4401584)
3K4M-4MZ	177.48/(14672942)	0.236/(6946726)
Zym-Cho8	—	0.037/(9291139)
Zym-Cho7	1522.8/(12133002)	0.05/(12133002)
Cho8-Lath	5122.8/(12133003)	—
Lath-7DeC	—	0.032/(3997841)
7DeC-Chol	—	1.1/(14453564)
Mean	7899	0.042 (excluding 7.7 and 1.14 as outliers)

Retrieved 27th October, 2009.

## 4 Estimated parameters

Interaction	Turnover (hr <sup>-1</sup> ) / (pubmed ID)	Michaelis-Menten Constant (mM) / (pubmed ID)
ACoA-HCoA	—	0.042
HCoA-M	7900	—
M-M5P	7900	—
IsPP-FPP	7900	0.042
23Ox-Lan	7900	—
Lan-44Di	7900	—
44Di-14De	7900	—
14De-4MZC	7900	0.042
4MZC-3K4M	7900	—
Des-Chol	7900	0.042
Zym-Cho8	7900	—
Cho8-Lath	—	0.042
Lath-7DeC	7900	—
7DeC-Chol	7900	—

Interaction	Mass action constant (hr <sup>-1</sup> )
4MZ-Zym	156
Cho7-7DeD	156
7DeD-Des	156

Interaction	Rate constant of competing interaction (hr <sup>-1</sup> ) - IFN $\gamma$ treatment
ACoA-HCoA	0.0134
HCoA-M	0.1977
M-M5P	0.1858
M5P-M5PP	8.8154
M5PP-IsPP	2.0107
IsPP-FPP	8.6358
FPP-Squa	15.5664
Squa-23Ox	0.0004
23Ox-Lan	0.3178
Lan-44Di	1.1174
44Di-14De	0.6450
14De-4MZC	6.7600
4MZC-3K4M	0.5712
3K4M-4MZ	0.0011
4MZ-Zym	1.5600
Zym-Cho7	0.2680
Cho7-7DeD	1.5600
7DeD-Des	1.5600
Des-Chol	0.1855
Zym-Cho8	0.2680
Cho8-Lath	1.3027
Lath-7DeC	1.3936
7DeC-Chol	0.0296

Interaction	Rate constant of competing interaction (hr <sup>-1</sup> ) - mCMV infection
ACoA-HCoA	0.00745
HCoA-M	0.18893
M-M5P	0.16232
M5P-M5PP	8.32940
M5PP-IsPP	1.71684
IsPP-FPP	8.57849
FPP-Squa	18.43532
Squa-23Ox	0.00003
23Ox-Lan	0.26313
Lan-44Di	0.77913
44Di-14De	0.60956
14De-4MZC	5.82151
4MZC-3K4M	0.31487
3K4M-4MZ	0.00127
4MZ-Zym	1.56000
Zym-Cho7	0.2008
Cho7-7DeD	1.56000
7DeD-Des	1.56000
Des-Chol	0.16598
Zym-Cho8	0.2008
Cho8-Lath	0.85392
Lath-7DeC	0.96270
7DeC-Chol	0.02307

## 5 Normalized enzyme activity time course following infection with mCMV.

Time (hr)	HMGCR	MVK	PMVK	MVD	FDPS	FDFT1	SQLE	DHCR7
0	258	76	874	111	7029	3425	486	495
0.5	253	68	855	106	6990	3322	428	436
1	255	54	790	91	6568	3509	490	339
1.5	271	38	735	76	6036	3346	515	279
2	267	35	639	65	5082	2942	530	297
2.5	271	39	590	70	4612	2411	483	280
3	259	47	541	66	4186	1861	462	259
3.5	287	44	524	64	4387	1674	466	175
4	293	50	515	68	4666	1445	396	215
4.5	314	51	501	74	5062	1341	375	231
5	304	66	522	80	4848	1154	304	296
5.5	304	64	535	71	4404	1022	309	322
6	290	77	550	73	3468	997	282	334
6.5	307	63	574	65	3335	1029	318	314
7	318	73	587	68	3224	1114	310	306
7.5	317	58	613	61	3573	940	281	282
8	300	62	580	67	3303	919	271	304
8.5	289	55	562	64	3070	825	260	266
9	286	66	580	65	2713	927	217	244
9.5	273	56	546	56	2516	895	207	219
10	254	42	517	45	2434	872	205	208
10.5	232	31	464	43	2233	840	243	215
11	212	39	446	48	1915	764	187	205
11.5	199	50	445	55	1516	731	154	193
12	196	66	459	67	1382	658	141	187
24	105	66	459	44	1639	1087	105	631

Time (hr)	HMGCS	LSS	CYP51A1	TM7SF2	SC4MOL	NSDHL	HSD17B7	DHCR24
0	1441	77	76	396	4770	43	261	136
0.5	1510	72	74	402	4570	44	253	117
1	1707	85	72	391	4931	52	254	115
1.5	1809	92	69	373	5256	63	258	108
2	1649	98	60	312	5158	68	242	102
2.5	1389	90	61	299	4859	72	250	97
3	1307	88	61	287	3901	79	238	91
3.5	1502	85	67	323	3688	77	255	89
4	1538	87	61	296	3320	59	216	84
4.5	1665	81	62	322	3169	52	208	84
5	1309	79	65	319	2887	58	173	89
5.5	1101	74	67	344	2359	68	169	90
6	853	71	65	314	2056	65	155	89
6.5	877	74	64	330	1875	64	169	84
7	928	74	66	341	1814	67	173	90
7.5	893	72	63	347	1832	63	173	90
8	799	68	55	319	1694	59	163	84
8.5	678	60	51	307	1615	56	160	77
9	628	57	50	293	1603	58	149	74
9.5	672	56	54	276	1689	63	151	79
10	710	59	52	260	1764	65	139	81
10.5	724	56	53	247	1659	66	150	76
11	605	53	53	248	1460	61	140	73
11.5	558	47	55	227	1428	56	139	63
12	574	52	63	225	1426	59	133	69
24	301	44	22	225	1334	21	149	140

Time (hr)	EBP	SC5DL
0	1079	601
0.5	1533	583
1	1505	664
1.5	1380	771
2	1258	809
2.5	1192	792
3	1277	693
3.5	1402	757
4	1402	734
4.5	1359	739
5	1182	623
5.5	1244	525
6	1272	452
6.5	1497	459
7	1628	500
7.5	1709	471
8	1778	465
8.5	1691	413
9	1655	435
9.5	1613	431
10	1647	463
10.5	1659	454
11	1493	417
11.5	1298	372
12	1224	359
24	1224	359

## 6 Normalized enzyme activity time course following treatment with IFN $\gamma$ .

Time (hr)	HMGCR	MVK	PMVK	MVD	FDPS	FDFT1	SQLE	DHCR7
0	270	87	925	130	7076	2892	677	635
0.5	296	75	902	134	6391	3508	647	577
1	277	83	886	149	7127	3302	768	680
1.5	320	84	1016	137	7821	3668	810	661
2	288	94	1014	140	7617	2795	811	753
2.5	286	74	932	109	5545	2561	648	568
3	245	64	821	96	4392	1956	539	537
3.5	247	55	872	69	4355	1934	464	423
4	271	66	1107	69	5263	1834	407	409
4.5	254	69	1193	72	5082	1678	375	372
5	258	87	1347	89	5306	1579	344	360
5.5	247	78	1299	87	4728	1419	326	323
6	241	85	1301	90	5479	1175	271	311
6.5	228	66	1190	81	5239	928	331	252
7	211	63	1169	81	5324	807	203	259
7.5	207	55	1110	75	4373	745	197	212
8	219	67	1003	88	3942	756	188	206
8.5	224	80	957	84	3840	694	172	168
9	219	80	834	79	3189	600	152	157
9.5	190	72	857	74	2811	515	159	162
10	174	57	789	64	2264	465	167	166
10.5	186	70	778	71	2227	527	200	178
11	186	69	679	60	1993	521	205	173
11.5	178	67	609	61	1833	496	202	182
12	156	58	602	62	1544	450	185	180
24	99	58	602	84	3870	1667	345	631

Time (hr)	HMGCS	LSS	CYP51A1	TM7SF2	SC4MOL	NSDHL	HSD17B7	DHCR24
0	2594	93	109	419	5539	78	227	152
0.5	2491	104	117	410	5657	89	242	131
1	2527	104	120	414	5593	74	270	138
1.5	1930	99	151	497	6129	70	324	122
2	1740	92	150	494	5924	63	326	123
2.5	1364	85	129	422	5303	68	247	105
3	1663	75	97	334	4205	59	201	89
3.5	1803	65	94	331	3805	51	185	77
4	1915	66	116	397	3919	50	224	84
4.5	1437	65	123	406	3693	50	226	90
5	1131	71	127	435	3439	61	219	97
5.5	966	65	120	421	3130	57	200	86
6	814	71	138	438	2694	66	186	85
6.5	581	64	145	425	2324	60	172	87
7	476	61	153	427	2028	63	159	92
7.5	500	55	146	420	1923	59	138	102
8	542	57	172	448	1849	60	146	99
8.5	545	57	202	475	1676	64	146	96
9	501	58	203	450	1714	66	153	89
9.5	513	56	175	420	1726	67	144	83
10	535	49	145	367	1811	60	130	77
10.5	607	58	109	358	1962	68	136	83
11	643	50	75	332	2218	63	122	67
11.5	662	50	52	313	2402	60	118	64
12	679	41	49	283	2421	57	101	55
24	1221	58	65	283	5596	80	136	140

Time (hr)	EBP	SC5DL
0	1646	870
0.5	1696	908
1	1815	911
1.5	2303	1026
2	2444	995
2.5	2033	899
3	1671	731
3.5	1610	694
4	1870	683
4.5	1944	662
5	1924	638
5.5	1914	657
6	2035	606
6.5	2202	511
7	2239	468
7.5	2233	460
8	2020	512
8.5	1953	499
9	1703	454
9.5	1703	378
10	1780	319
10.5	1820	302
11	1902	290
11.5	1805	274
12	1848	243
24	1848	243

## 7 Calculating initial conditions

The most general case is an interaction in which the substrate is consumed in a Michaelis-Menten interaction and an off-pathway, competing mass action interaction. If  $F$  is the rate at which a substrate is formed, the pathway will be at dynamic equilibrium if

$$F = \frac{k_{cat}ES}{k_m + S} + k_bS$$

where  $k_b$  is the mass action rate constant for the off-pathway interaction. After some rearrangement, this yields the following quadratic equation

$$0 = k_bS^2 + (k_bk_m + k_{cat}E - F)S - Fk_m$$

which, from the monotonicity of the mass action term and the Michaelis-Menten terms, can be seen to have one positive solution.

Where an interaction is mass action in form, we have dynamic equilibrium when

$$F = k_{autocat}S + k_bS$$

This can be rearranged to

$$S = \frac{F}{k_{autocat} + k_b}$$

Zymosterol is consumed in two Michaelis-Menten interactions. Here, dynamic equilibrium is established when

$$F = \frac{k_{cat}^1 E^1 S}{k_m^1 + S} + \frac{k_{cat}^2 E^2 S}{k_m^2 + S} + k_bS$$

After some rearrangement, this yields the following cubic equation

$$\begin{aligned} 0 &= k_bS^3 \\ &\quad (k_bk_m^1 + k_bk_m^2 + k_{cat}^2E + k_{cat}^1E - F)S^2 \\ &\quad (k_m^2k_m^1k_b + k_c^1Ek_m^2 + k_c^2Ek_m^1 - Fk_m^1 - Fk_m^2)S \\ &\quad - Fk_m^1k_m^2 \end{aligned}$$

which, from the monotonicity of the two Michaelis-Menten terms and the mass action term, can be seen to have one positive solution.

## 8 Metabolite levels at 0, 12 and 24 hours post infection or post treatment

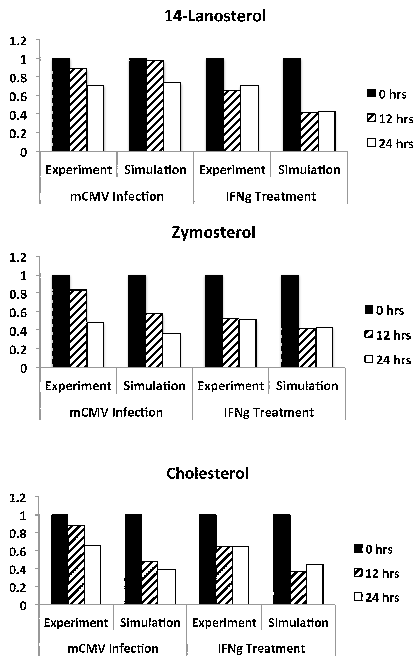


**Figure 1: Metabolite levels at 0, 12 and 24 hours post infection or post treatment.** The normalized concentrations of 14-Lanosterol, Zymosterol and Cholesterol at 0 hours (solid, black), 12 hours (diagonal stripes) and 24 hours (open boxes) after mCMV infection and after IFN $\gamma$  treatment. We show results from experiment and simulation. Experimental measurements were normalized against measurements from a mock time course and simulated measurements were normalized against the concentration at 0hrs.

## 9 Inhibitor levels responsible for the flux profile in Fig. 4B

Interaction	Inhibitor to $K_i$ ratio
ACoA-HCoA	22.94
HCoA-M	23.97
M-M5P	23.91
M5P-M5PP	24.00
M5PP-IsPP	23.98
IsPP-FPP	24.00
FPP-Squa	24.00
Squa-23Ox	23.57
23Ox-Lan	23.98
Lan-44Di	23.99
44Di-14De	24.00
14De-4MZC	24.00
4MZC-3K4M	23.99
3K4M-4MZ	23.87

## 10 Flux profiles from 0 to 24 hours post IFN $\gamma$ treatment

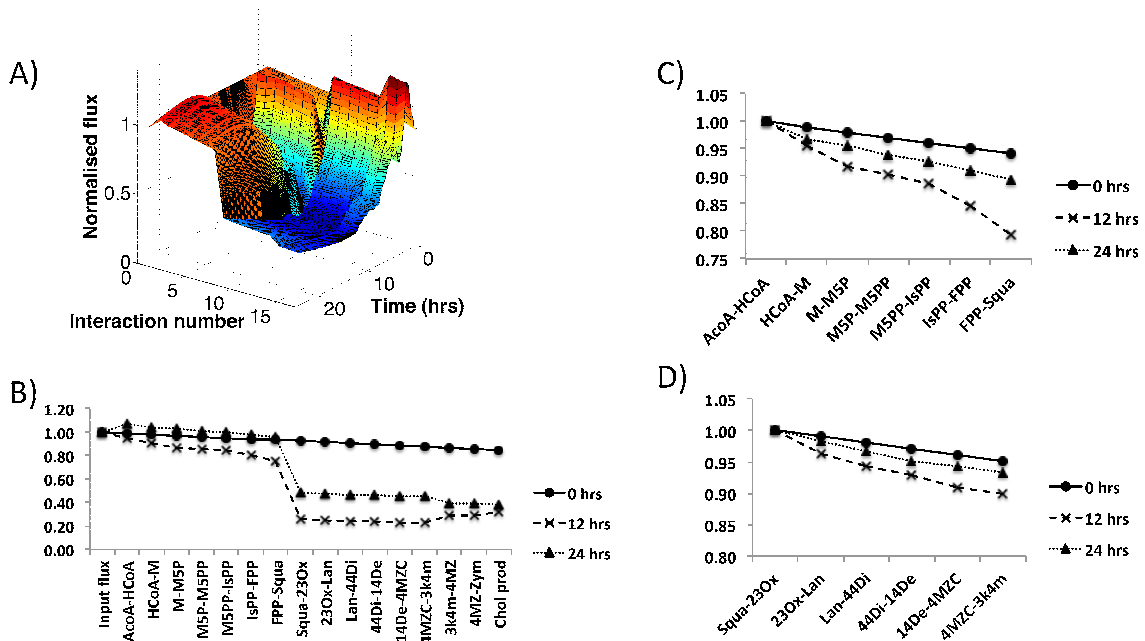


**Figure 2: Flux profiles from 0 to 24 hours post IFN $\gamma$  treatment.** The flux through the cholesterol biosynthesis pathway following treatment with IFN $\gamma$ . A) The development of the flux through the pathway in simulation is shown from 0 hrs to 24 hrs following treatment. Interactions are numbered from 1 (the input flux) to 17 (cholesterol production). For the full numbering, see Supplementary section 12. At 0 hrs, the flux through the pathway is relatively constant. However, by 12 hrs the flux has been significantly suppressed along the pathway. By 24 hrs, the pathway has started to show a modest recovery. B) The profile of flux through the pathway at 0 hrs, 12 hrs and 24 hrs following treatment. These profiles represent cross sections of the surface shown in A). The flux is dramatically reduced in the first 12 hrs with a modest increase occurring between 12 and 24 hrs following treatment. Interactions can be classified as dominant (Squa-23Ox) and non-dominant (the remainder) depending on their degree of impact on the pathway flux. C) The flux through the non-dominant interactions between ACoA-HCoA and FPP-Squa, normalized against the flux through the ACoA-HCoA interaction. D) The flux through the non-dominant interactions between Squa-23Ox and 4MZC-3K4M normalized against the flux through the interaction Squa-23Ox.

## 11 Flux profiles from 0 to 24 hours post mCMV infection

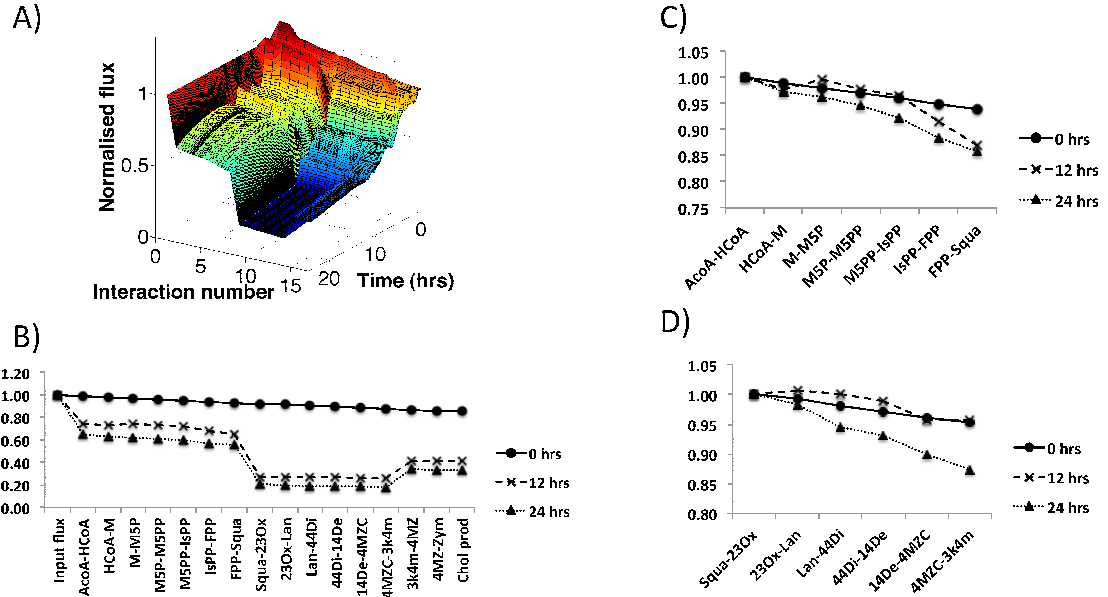


**Figure 3: Flux profiles from 0 to 24 hours post mCMV infection.** The flux through the cholesterol biosynthesis pathway following infection with mCMV. A) The development of the flux through the pathway in simulation is shown from 0 hrs to 24 hrs post infection. Interactions are numbered from 1 (the input flux) to 17 (cholesterol production). For the full numbering, see Supplementary section 12. At 0 hrs, the flux through the pathway is relatively constant. However, by 24 hrs the flux has been significantly suppressed along the pathway. B) The profile of flux through the pathway at 0 hrs, 12 hrs and 24 hrs post infection. These profiles represent cross sections of the surface shown in A). The flux is dramatically reduced in the first 12 hrs with a further reduction occurring between 12 and 24 hrs following infection. Interactions can be classified as dominant (ACoA-HCoA and Squa-23Ox) and non-dominant (the remainder) depending on their degree of impact on the pathway flux. C) The flux through the non-dominant interactions between ACoA-HCoA and FPP-Squa, normalized against the flux through the ACoA-HCoA interaction. The flux through these non-dominant interactions shows a mild suppression between 0 hrs and 12 hrs, but a more significant suppression between 12 hr sand 24 hrs. D) The flux through the non-dominant interactions between Squa-23Ox and 4MZC-3K4M normalized against the flux through the interaction Squa-23Ox. The flux through these interactions shows no suppression between 0 hrs and 12 hrs, but a significant suppression between 12 hrs and 24 hrs.

## 12 Interaction numbering

1	Input flux
2	AcoA-HCoA
3	HCoA-M
4	M-M5P
5	M5P-M5PP
6	M5PP-IsPP
7	IsPP-FPP
8	FPP-Squa
9	Squa-23Ox
10	23Ox-Lan
11	Lan-44Di
12	44Di-14De
13	14De-4MZC
14	4MZC-3k4m
15	3k4m-4MZ
16	4MZ-Zym
17	Cholesterol production (7DeC-Chol + Des-Chol)